Mechanics of kerf patterns for creating freeform structures

Renzhe Chen, Coby Turman, Mingliang Jiang, Negar Kalantar, Michael Moreno & Anastasia Muliana

Acta Mechanica

ISSN 0001-5970 Volume 231 Number 9

Acta Mech (2020) 231:3499-3524 DOI 10.1007/s00707-020-02713-8



Your article is protected by copyright and all rights are held exclusively by Springer-Verlag GmbH Austria, part of Springer Nature. This eoffprint is for personal use only and shall not be self-archived in electronic repositories. If you wish to self-archive your article, please use the accepted manuscript version for posting on your own website. You may further deposit the accepted manuscript version in any repository, provided it is only made publicly available 12 months after official publication or later and provided acknowledgement is given to the original source of publication and a link is inserted to the published article on Springer's website. The link must be accompanied by the following text: "The final publication is available at link.springer.com".



Author's personal copy

Acta Mech 231, 3499–3524 (2020) https://doi.org/10.1007/s00707-020-02713-8



ORIGINAL PAPER

Renzhe Chen · Coby Turman · Mingliang Jiang · Negar Kalantar · Michael Moreno · Anastasia Muliana

Mechanics of kerf patterns for creating freeform structures

Received: 21 November 2019 / Revised: 26 March 2020 / Published online: 24 June 2020 © Springer-Verlag GmbH Austria, part of Springer Nature 2020

Abstract A relief cutting method, or kerfing, is considered to create flexible freeform surfaces from relatively stiff and thick panels. The flexibility and moldability are achieved by introducing slender components within the panel, forming kerf patterns, and hence reducing the second moment and polar moment of an area of the solid panel. This paper presents a systematic study on the deformations of kerf unit-cells and of kerf panels. Two different kerf patterns, i.e., square and hexagon, with various cut densities are studied. The effects of different cutting density and kerf patterns on the stretching, bending, and twisting deformations are examined. Understanding the influence of kerf patterns and cut densities on various deformation mechanisms will guide the design of freeform complex shapes out of kerf panels. Experimental tests were performed on unit-cells under different boundary conditions, e.g., uniaxial and biaxial stretching and bending. The tests were also performed on kerf panels with different kerf patterns and varying cut densities. We used a nonlinear beam element in order to describe the deformations of the slender components within the kerf patterns. We compared the overall deformations in the kerf unit-cells and panels from the beam element model and experimental tests. Using the kerfing technique allows for generating flexible structures with complex geometries from massproduced panels of standard shape and size. When using the kerfing method to achieve the desired surface topology, the stresses, strains, and displacements in the surface will depend on the kerf pattern, cut density, and constituent behavior.

1 Introduction

With recent advances in differential geometry, computational geometry, and computer graphics, various forms of complex shapes can be designed which push further architectural design beyond simple geometries. For example, Pottmann et al. [17] presented a computational method based on parallel meshes in creating freeform structures comprising of arrangements of prismatic beams. Postle [16] utilized the concept of pair of splines within developable surfaces for generating curved structures from folding of planar sheet materials. Andrade et al. [1] proposed an automatic generation of cladded panels of honeycomb patterns with directional variation and spatial scale in order to create surfaces with complex shapes. The honeycomb patterns give flexibility in shaping the geometry. Despite advances in computational and design tools for generating freeform structures, several challenges still remain with regard to constructing such complex structures. There are currently limited materials, i.e., steel, concrete, wood, aluminum, and glass, which are suitable for building constructions. These materials possess sufficient strength for structural integrity, but they are relatively stiff making it difficult to

R. Chen \cdot C. Turman \cdot M. Jiang \cdot M. Moreno \cdot A. Muliana (\boxtimes) Department of Mechanical Engineering, Texas A&M University, College Station, USA E-mail: amuliana@tamu.edu

N. Kalantar



Fig. 1 Flexible kerf MDF panel from originally rigid panel

form them into complex shapes. Even when it is possible to form complex shapes like in sheet metal forming, the cost of fabricating individual panels of unique shapes is extremely high. For materials that are fabricated with molds, the idea of reusable molds will potentially reduce the construction cost and waste. However, the reusable mold is still labor intensive. The complexity in generating freeform shapes is further alleviated by the large variations in the mechanical and non-mechanical behaviors of different materials. It is then necessary to simultaneously perform structural analyses while designing complex freeform structures.

One of the practical methods to create flexible surfaces from relatively stiff planar materials like metals, wood, and medium-density fiberboard (MDF) is relief cutting or kerfing. This approach allows for utilizing mass-produced materials of standard shape and size in generating flexible surfaces with complex geometries. The mechanism is based on introducing slender components within the panel, forming kerf patterns, and hence reducing the second moment and polar moment of an area of the solid panel. The out-of-plane deformations in the kerf panels are dominated by bending and twisting of the cut components in different directions. Figure 1 illustrates several examples of shape reconfigurations in a kerf panel out of MDF. There have been several kerfing patterns currently available. Ivanišević [10] designed an interlocked Archimedean spirals pattern, which can form double curvature panels. Hoffer et al [9] and Kalantar and Borhani [12], taking the advantage of wooden properties, used the kerfing of wood to design of a curved pavilion. Bending of the corners is achieved due to the compliant characteristics in the kerf regions. Based on the 2D meander pattern, Zarrinmehr et al. [24] used a remeshing method to develop an algorithm for generating more general shapes of kerf pattern, in which local properties of these patterns can be controlled to acquire the desired stiffness. A similar approach has also been done by Greenberg and Korner [6], where they created planar structures with variable stiffness by varying the cut density gradients. Guzelci et al. [8] investigated different methods and cut patterns of planar materials in achieving bending (curvature changes). They focused on the geometrical aspects and aimed to determine correlations between bending behaviors and geometrical parameters. It was concluded that the topological cut patterns played an important role in determining bending and flexibility of the planar surface. In addition to the geometrical aspects, the mechanical behaviors of the planar materials are crucial in determining the flexibility/bending of the structures, which so far has not been considered. The same cut patterns done on MDF and aluminum plates of the same geometrical parameters will lead to different deformation behaviors.

Although there have been several studies on utilizing the kerfing method to create flexible structures in architecture and construction field, a systematic investigation on the mechanics of kerf structures is still lacking. This paper presents a systematic study on the deformations in the unit-cells of kerf systems that experience stretching, bending, and twisting. The effects of different cutting density and kerf patterns on the deformations of the unit-cells are examined. Mechanical tests on unit-cells of two kerf patterns with different cut densities are also performed. It is then possible to attain various deformed configurations in kerf panels by arranging the unit-cells with different densities in forming flexible panels. We then present designs and analyses of curved structures out of kerf panels. Some of the kerf panels are tested to examine their overall deformations. With understanding the unit-cell deformations and arranging them in different orders and configurations, designers could predict the final shape of the panels after prescribing forces. A more comprehensive study can also include design optimization for the kerf patterns and cut densities in order to achieve freeform complex geometries.

Recent studies on using metamaterials by Zehnder et al. [25], Konakovic-Lukovic et al. [14], and Guseinov et al. [7] present programmable surfaces that can be reconfigured from a planar surface. In Guseinov et al. [7], the design criteria include both temporal and spatial variations, and the deformations are achieved by non-mechanical stimuli. Including the design optimization is beyond the scope of this study.

2 Kerfing patterns on medium-density fiberboard (MDF) panels

In this study, we consider two cut patterns, i.e., square interlocked Archimedean spiral and hexagon spiral, see Figs. 2 and 3. The advantage of these patterns is that they are relatively easy to arrange to form flexible panels in order to achieve desired freeform shapes. A relatively stiff flat panel of MDF is used. The thickness of the panel is 0.125 inches. The MDF is formed by chopped wood fibers that are pressed together and bonded with polymeric resin. Their in-plane mechanical properties can be considered isotropic. The mechanical properties in the panel thickness direction might be different than the in-plane properties, as suggested by the numerical simulations of microstructures of MDF [21]. However, there have been no experimental data on the mechanical properties of MDF fibers in the thickness directions. The basic mechanical properties of the MDF panel, obtained from the manufacturer, are as follows: the extensional (elastic) modulus is 580 ksi (4 GPa), Poisson's ratio is 0.25, the tensile strength is 2.6 ksi (18 MPa), and the ultimate tensile strain is 0.5%. In this study the MDF is considered as a linear elastic isotropic material, and hence, the shear modulus is 232 ksi (1.6 GPa). It is noted that in Fig. 2 (left) the sharp corners result in breaking of the cut patterns (shown by yellow arrows), which are more pronounced for the pattern with higher cut density. This is due to high stress concentrations occurring in the regions with a relatively small cross-sectional area and sharp junction. In order to mitigate the stress concentration effect, a square kerfing pattern with a fillet radius at the junction is considered (shown with a red arrow in Fig. 2 right).

While kerfing technique promotes flexible surfaces, it generally reduces the load carrying ability of the panels. Higher density cuts lead to more flexible and lower load bearing systems. When designing desired geometrical shapes, we can consider the kerf panels with distributions of cut densities to have a balance between flexibilities and load bearing. For this purpose, we study unit-cells of the same pattern with different cut densities, see Figs. 2 and 3. These different densities are named as low density (LD), medium density (MD), and high density (HD), associated with the number of the cutline layers in a unit-cell model. The LD cell has the lowest number of cut lines, while the HD cell has the highest number of cut lines. The unit-cells with square cut pattern have the side length of 1 inch and the thickness of 0.125 in. Fillets of 0.02 in. radius are included to these unit-cell models for all corners in order to improve their performance by avoiding failure at the junctions (sharp corner). The unit-cells with hexagon pattern have the side length of 1 in. and thickness of 0.125 in. In all unit-cells, the kerfing patterns are formed by arrangements of straight prismatic bars with a rectangular cross section. The pattern with HD cut leads to slenderer bars with a relatively small cross-sectional area, low second moments and polar moment of an area, and low torsional rigidity, resulting in more compliant behaviors.

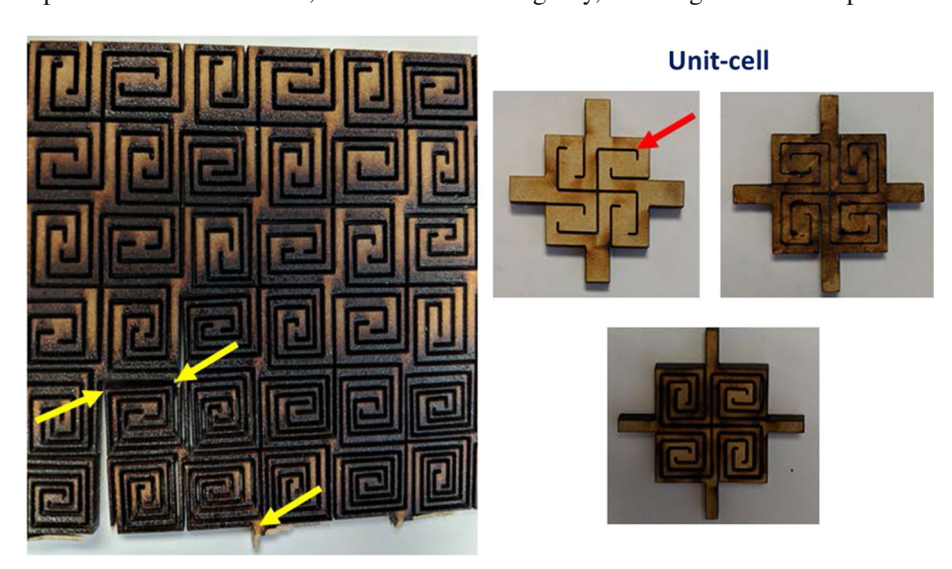


Fig. 2 Square interlocked Archimedean spiral pattern on an MDF panel (left); unit-cells with different cut densities (right)

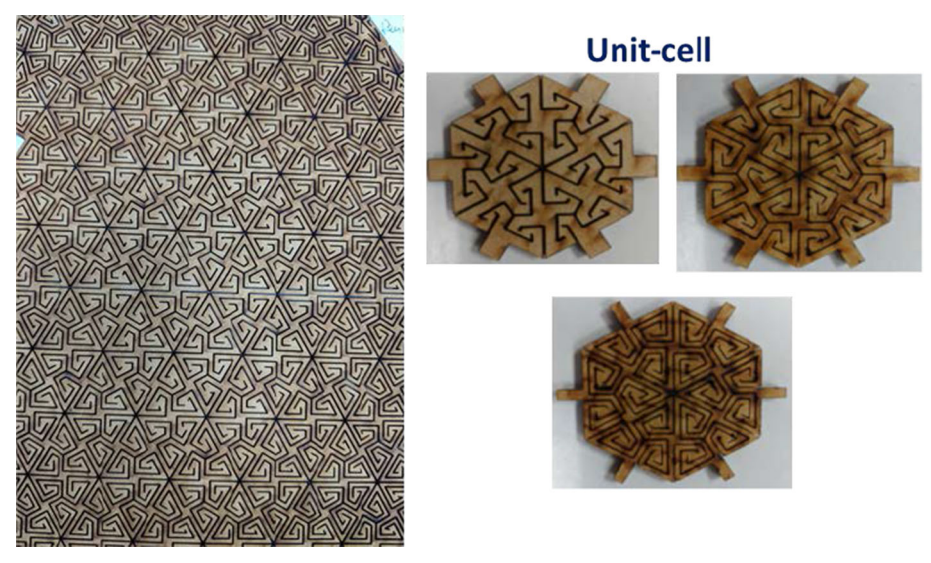


Fig. 3 Hexagonal spiral pattern on MDF panel (left); unit-cells with different cut densities (right)

3 Experimental tests

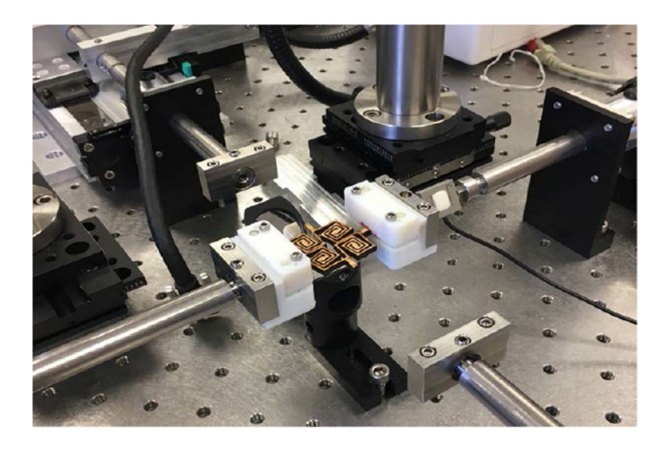
A custom-built mechanical testing system is used to perform the uniaxial, biaxial, and bending tests on the unit-cell specimens, see Fig. 4. Motorized linear actuators (DS4 series, Kollmorgen Corp., Radford, VA), each equipped with a 10-mm lead and coupled with a servomotor (AKM23D, Kollmorgen Corp., Radford, VA. Each servomotor (AKM23D, Kollmorgen Corp., Radford, VA), are driven by a servo drive (AKD-P00306, Kollmorgen Corp., Radford, VA) in order to provide displacements. A 100-lbs load cell (Honeywell Sensotec, Model 31, Columbus, Ohio) is used to measure the load. A +/- 2-inch linear variable differential transformer (Honeywell Sensotec, MVL7C, Columbus, Ohio) is used to measure the axial displacement. The system is able to perform both load and displacement control. A custom-designed serrated clamp was used to grip the specimens.

One arm of the specimen was fixed, while the opposite arm was stretched by the linear actuator in order to perform a uniaxial test. Three measurements on the initial grip distance were taken after the specimen was mounted, and an average was calculated. Ink was marked at the clamping sites to check slippage. For each pattern, three specimens were tested until failure. Two of them were stretched at a displacement rate of 0.015 in/s, and one was at a displacement rate of 0.0015 in/s. There were no apparent differences in the responses from these two rates, as will be seen later in the experimental results. The remaining tests were done at the displacement rate of 0.015 in/s. For the biaxial test, all the four arms were simultaneously stretched along the axes' directions. For the bending test, the specimen was rotated so that the plane normal direction was in the direction of the rod axis. Two arms were gripped, and the rod pushed the center of the panel (see Fig. 4). The unit-cells of the square pattern were subjected to uniaxial, biaxial, and bending tests, while the unit-cells with the hexagon pattern were subjected to uniaxial and bending tests.

We also performed a bending test on kerf panels with square and hexagon kerf patterns in order to create a dome shape. The testing setup is shown in Fig. 5. The same device was used for testing with custom-built grips and push rod to deform the center of the panel.

4 Modeling and simulation

In order to analyze the deformations of the kerf unit-cells and panels, we consider representing the segments (prismatic bars) in the kerf systems with beam elements of a solid rectangular cross section, see the illustration in Fig. 6. The side length *s* is equal to 1 inch. The actual unit-cell model is generated using 3D continuum finite elements, while the simplified model is generated using beam finite elements. Each beam has a thickness of 0.125 in, which is the thickness of the MDF panel, and the width of the beam depends on the cut density and pattern of the kerf panel. The width of the beam is defined based on the number of cutline and the gap from laser cutting the specimen, which is around 0.025 in. Tables 1 and 2 present the cross-sectional dimensions



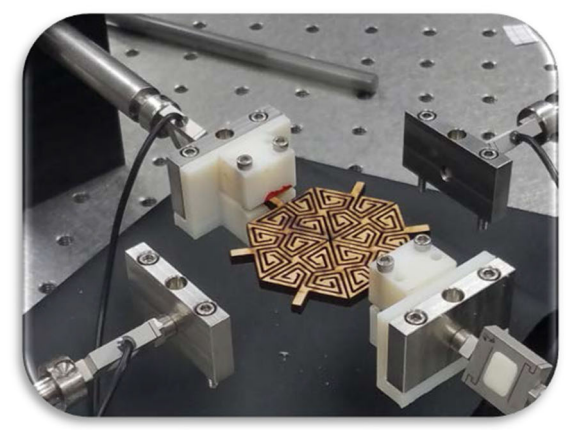




Fig. 4 Experimental test setup for unit-cells

of the beam for the square and hexagon patterns with different cut densities. Depending on the deformations prescribed to the unit-cell and panels, each beam can experience axial stretching, transverse shearing, bending, and/or twisting. For example, when uniaxial and biaxial loadings are imposed on the unit-cells, each beam is subjected to axial stretching, transverse shear, and/or bending about the out-of-plane axis. When the unit-cell is subjected to bending, each beam can experience transverse shearing, bending about the in-plane axis, and/or twisting. Table 3 depicts illustrations of local deformations of a unit-cell under different loading conditions. For a relatively slender beam, i.e., the length is much larger than the cross-sectional dimension, the contribution of the transverse shear deformation is negligible.

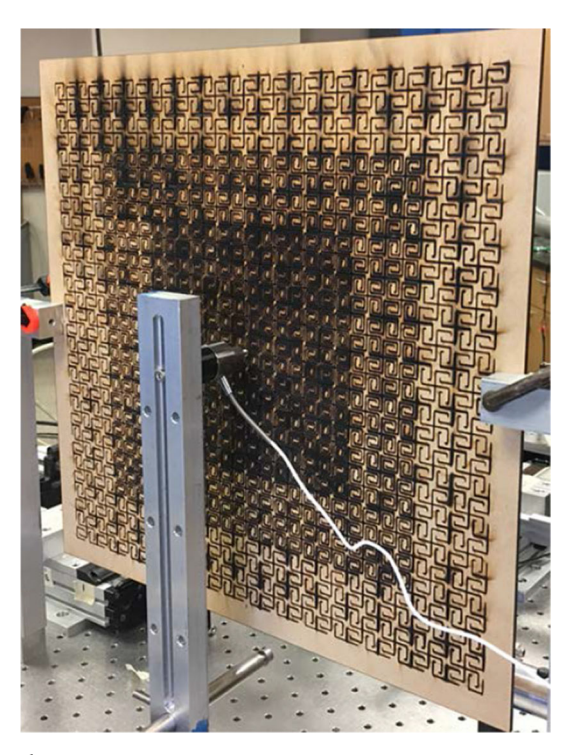
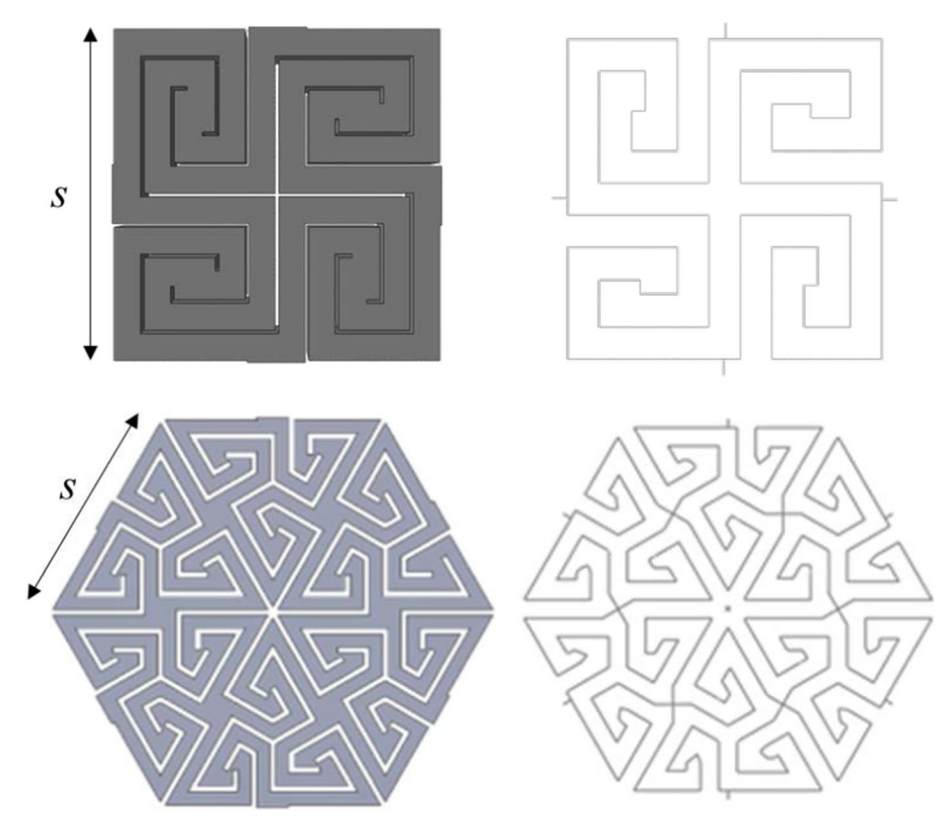


Fig. 5 Bending test of the kerf panel



 $\textbf{Fig. 6} \ \ \text{Geometrical models for square and hexagonal unit-cell (MD pattern)}. \ \ \text{The actual unit-cell model using 3D continuum (left) and the simplified model using beam (right) elements$

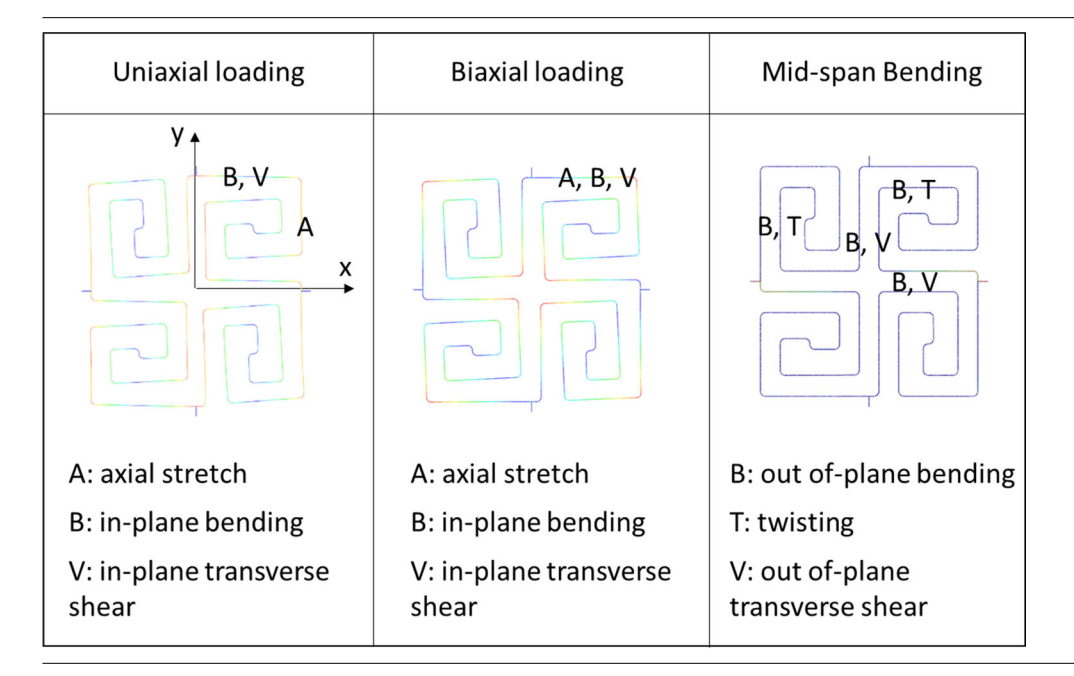
Table 1 Geometrical properties of the beam cross sections in unit-cells with a square pattern

Unit-cell	Area (in ²)	Second moment of area $I_{11} (\times 10^5 \text{ in}^4)$	Second moment of area $I_{22} (\times 10^{-5} \text{ in}^4)$	Polar moment of area $I_p (\times 10^{-5} \text{ in}^4)$
LD	0.125×0.1000	1.0417	1.6276	0.3073
MD	0.125×0.0583	0.2064	0.9489	0.1305
HD	0.125×0.0375	0.0549	0.6104	0.0782

Table 2 Geometrical properties of the beam cross sections in unit-cells with a hexagon pattern

Unit-cell	Area (in ²)	Second moment of area $I_{11} \times 10^{-5} \text{ in}^4$	Second moment of area $I_{22} (\times 10^{-5} \text{ in}^4)$	Polar moment of area $I_p (\times 10^{-5} \text{ in}^4)$
LD	0.125×0.1000	1.0417	1.6276	0.3073
MD	0.125×0.0633	0.2642	1.0303	0.1453
HD	0.125×0.0450	0.0949	0.7324	0.0956

Table 3 Local deformations of beam segments in square unit-cell of medium-density cut



4.1 Beam element model

We consider a general beam element that can undergo axial stretching, transverse shearing, bending about two lateral axes, and twisting. Depending on the density of the cut, some beam can be considered slender in which the transverse shear deformation is negligible, while some can form a thick section where the influence of transverse shear strain on the lateral deformations cannot be ignored. As will be discussed later, in the LD unit-cells some regions form a stocky section, which cannot be represented by a beam element. It is also noted that the beam elements, depending on their locations and loading conditions, can experience large deformations, mainly due to rotations. Even when undergoing large deformations, the strain or stretch of the material elements along the beam is rather small due to the use of MDF which has a relatively high elastic modulus. For references on the formulations of beam elements undergoing large deformations, governed by rotations, the readers can refer to Simo (1985), Reissner [18], Saje and Srpcic [19], Irschik and Gerstmayr [11], and Cesarek et al. [3].

The kinematics representation of the beam in the undeformed and deformed configurations is given in Fig. 7. The position of point P in the beam, in an undeformed configuration, is given as:

$$\mathbf{X}(S) = \mathbf{X}_{o}(S) + S_{1}\mathbf{T}_{1}(S) + S_{2}\mathbf{T}_{2}(S)$$
(1)

where $\mathbf{X}_o(S)$ is the position of the centerline of the beam along the arc length S. The planes through $\mathbf{X}_o(S)$ normal to \mathbf{N} are the cross section of the beam. A fiber within the cross section is defined by the unit vector fields $\mathbf{T}_1(S)$ and $\mathbf{T}_2(S)$, and $\{\mathbf{N}(S), \mathbf{T}_1(S), \mathbf{T}_2(S)\}$ is an orthonormal frame, where $\mathbf{N} = \mathbf{T}_1 \times \mathbf{T}_2$. Here \mathbf{N} is the normal unit vector to the cross section, and in the undeformed state, it is tangent to the line of the centerline $\mathbf{X}_o(S)$. Also S_1 and S_2 are the lateral axes of the beam cross section, and S_3 is the axial axis of the beam. The corresponding curvatures \mathbf{K}_1 , \mathbf{K}_2 , and twist \mathbf{T} in the undeformed configuration are then defined by:

$$K_1 = \mathbf{N} \cdot \frac{d\mathbf{T}_1}{dS}; \quad K_2 = \mathbf{N} \cdot \frac{d\mathbf{T}_2}{dS},$$
 (2)

$$T = -\mathbf{T}_1 \cdot \frac{\mathbf{dT}_2}{\mathbf{dS}} = \mathbf{T}_2 \cdot \frac{\mathbf{dT}_1}{\mathbf{dS}}.$$
 (3)

For an initially straight and untwisted beam, the unit-vector fields remain constant with the length S, and therefore, $K_1 = K_2 = T = 0$.

In the deformed configuration, the position of point P is given as:

$$\mathbf{x}(S) = \mathbf{x}_{o}(S) + S_{1}\mathbf{t}_{1}(S) + S_{2}\mathbf{t}_{2}(S) + w(S)\varphi(S_{1}, S_{2})\mathbf{n}(S)$$
(4)

where $\mathbf{x}_o(S)$ is the position of the centerline of the deformed beam. The unit vector \mathbf{n} is normal to the cross section of the deformed beam, and it is not tangent to $\mathbf{x}_o(S)$, and $\mathbf{n} = \mathbf{t}_1 \times \mathbf{t}_2$, where fibers within the cross section of the deformed configuration are defined by the unit vector fields $\mathbf{t}_1(S)$ and $\mathbf{t}_2(S)$. It is assumed that the fiber within the cross section of the beam does not experience stretch and only a fiber along the longitudinal axis of the beam experiences stretch. The last term of Eq. (4) is the contribution of warping in case of twisting of a noncircular cross section. Here w(S) is the warping amplitude; $\varphi(S_1, S_2)$ is the warping function of the cross section. From the vector position in Eq. (4), we can then determine the axial stretch along the centerline λ , transverse shear strains γ_1^s , γ_2^s , twist τ , curvatures κ_1 , κ_2 , and bicurvature χ as follows:

$$\lambda = \left| \frac{\mathrm{d}\mathbf{x}_o}{\mathrm{d}S} \right|,\tag{5}$$

$$\gamma_1^s = \lambda^{-1} \frac{\mathrm{d}\mathbf{x}_o}{\mathrm{d}S} \cdot \mathbf{t}_1; \quad \gamma_2^s = \lambda^{-1} \frac{\mathrm{d}\mathbf{x}_o}{\mathrm{d}S} \cdot \mathbf{t}_2, \tag{6}$$

$$\tau = -\mathbf{t}_1 \cdot \frac{\mathrm{d}\mathbf{t}_2}{\mathrm{d}S} = \mathbf{t}_2 \cdot \frac{\mathrm{d}\mathbf{t}_1}{\mathrm{d}S},\tag{7}$$

$$\kappa_1 = \mathbf{n} \cdot \frac{\mathrm{d}\mathbf{t}_1}{\mathrm{d}S}; \quad \kappa_2 = \mathbf{n} \cdot \frac{\mathrm{d}\mathbf{t}_2}{\mathrm{d}S},$$
(8)

$$\chi = \frac{\mathrm{d}w}{\mathrm{d}S}.\tag{9}$$

For a solid cross section, twisting is not from a distributed torque; the bicurvature, which is an axial strain variation along the centerline due to warping, is zero. From Eqs. (7) and (8), we can write:

$$\frac{\mathrm{d}\mathbf{t}_1}{\mathrm{d}S} = -\kappa_2 \mathbf{n} + \tau \mathbf{t}_2; \quad \frac{\mathrm{d}\mathbf{t}_2}{\mathrm{d}S} = \kappa_1 \mathbf{n} + \tau \mathbf{t}_1. \tag{10}$$

Finally, the displacements of point P can be determined by $\mathbf{u} = \mathbf{x} - \mathbf{X}$.

In order to determine the strains in the beam, we obtain the deformation gradient **F** as follows:

$$\mathbf{F} = \frac{d\mathbf{x}}{dS} \frac{dS}{d\mathbf{X}} + \frac{d\mathbf{x}}{dS_1} \frac{dS_1}{d\mathbf{X}} + \frac{d\mathbf{x}}{dS_2} \frac{dS_2}{d\mathbf{X}}.$$
 (11)

Once the deformation gradient is defined, we can determine the axial and shear strains in the beam element. In this study, we consider MDF kerf panels. The material stiffness of MDF is relatively high, in which the fibers within the cross section and along the beam longitudinal axis experience a relatively small stretch. The

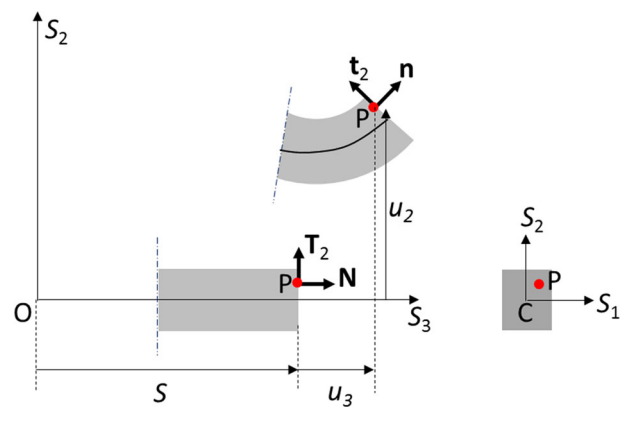


Fig. 7 Kinematic representation of a beam element in undeformed and deformed configurations

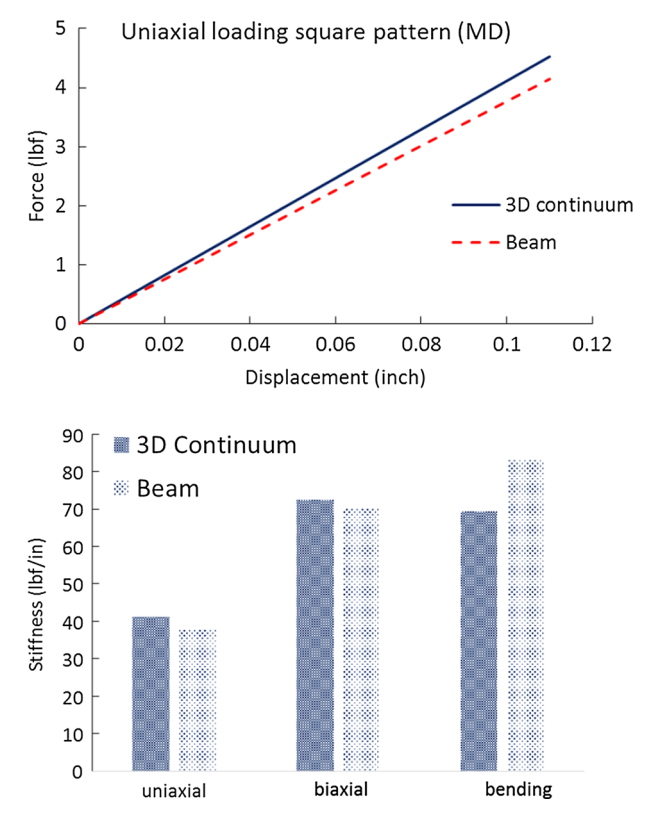


Fig. 8 Square pattern comparisons

beams within the kerf unit-cell and panel can undergo large deformations, which are dominated by the large curvature (large rotation). The axial stretch along the centerline is $\lambda \approx 1$.

The axial and shear strains in the beam with regard to the beam local cross-sectional normal and lateral directions are given as:

$$\varepsilon = \varepsilon_{33} = (\lambda - 1) - \frac{1}{\lambda} S_1 (\kappa_2 - K_2) + \frac{1}{\lambda} S_2 (\kappa_1 - K_1) + \frac{1}{\lambda} \chi \varphi (S_1, S_2),$$

$$v_1 = v_{21} = v_{32}^s + v_{12}^t = v_{12}^s + v_{12}^t$$
(12)

$$\gamma_{1} = \gamma_{31} = \gamma_{31}^{s} + \gamma_{31}^{t} = \gamma_{1}^{s} + \gamma_{1}^{t},
\gamma_{2} = \gamma_{32} = \gamma_{32}^{s} + \gamma_{32}^{t} = \gamma_{2}^{s} + \gamma_{2}^{t}$$
(13)

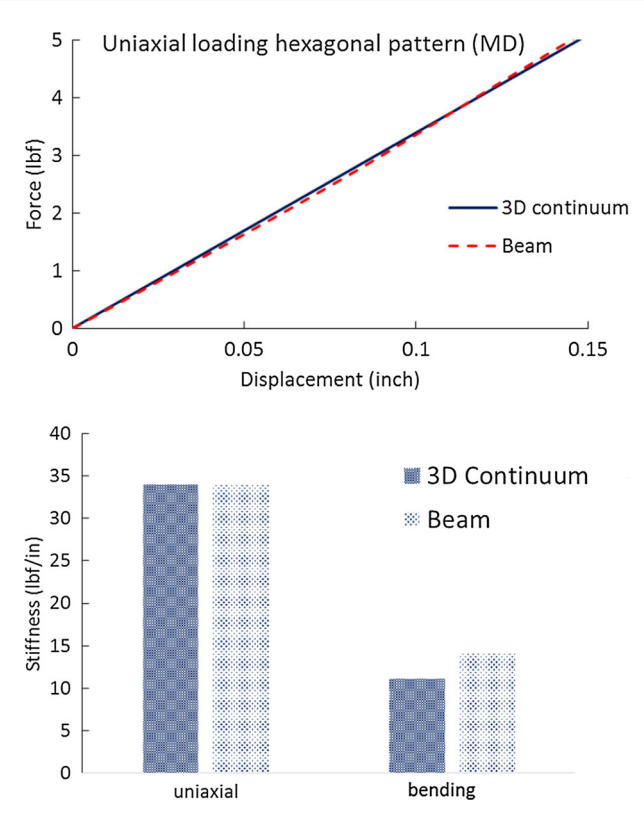


Fig. 9 Hexagonal pattern comparisons

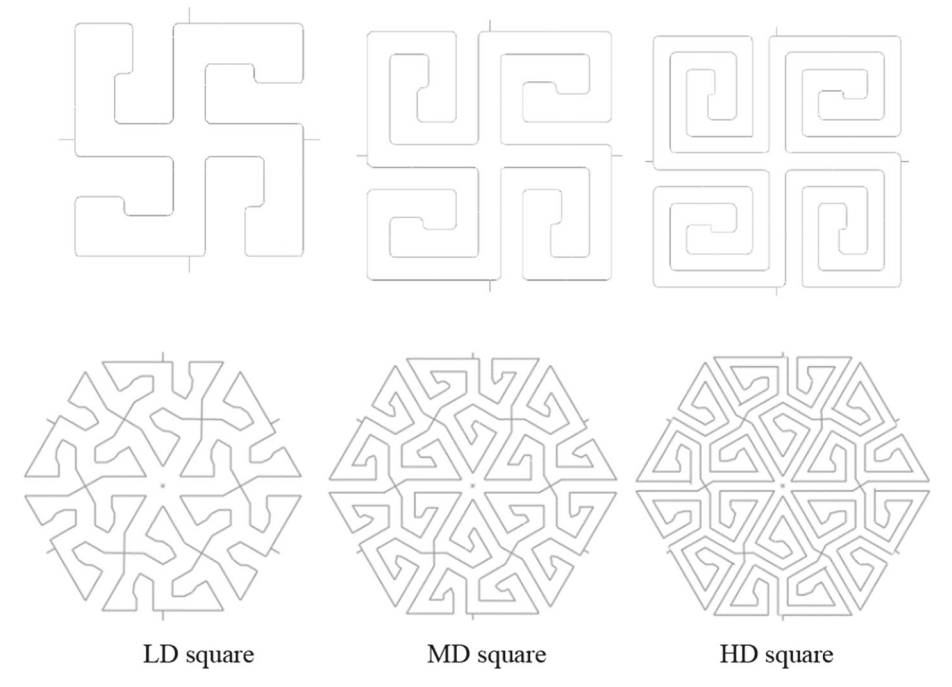


Fig. 10 Models for LD, MD, and HD unit-cells using beam elements

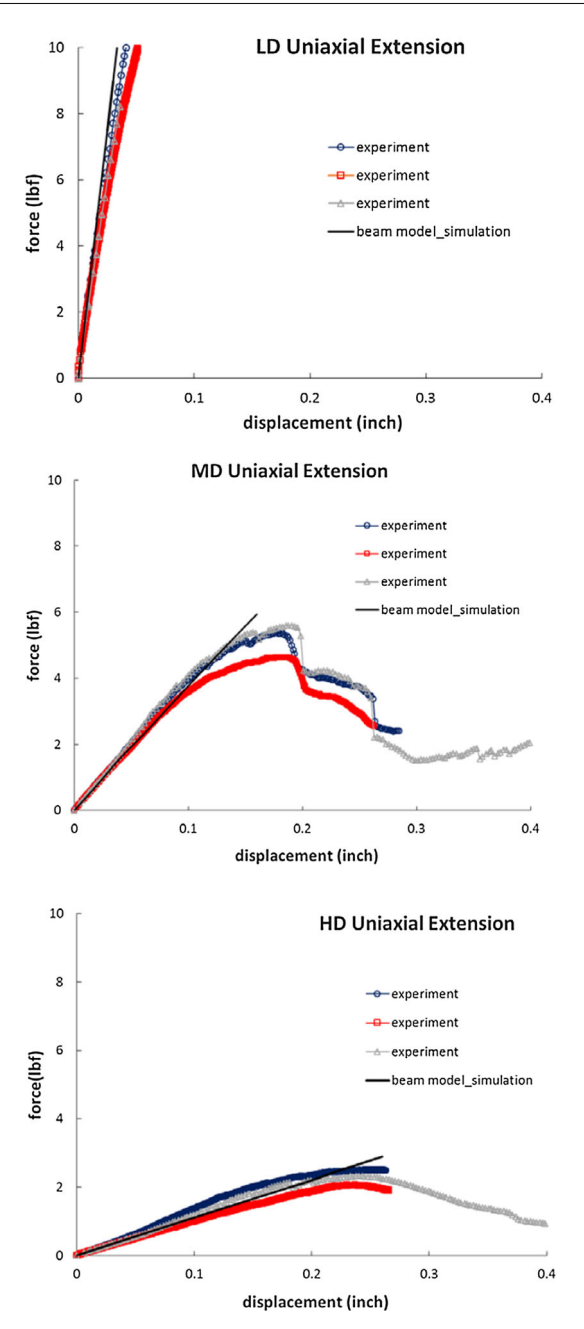


Fig. 11 Uniaxial responses of the square unit-cells

where the shear strains due to the transverse shear deformation are given in Eq. (6) and the shear strains due to twisting are composed of the components from free warping and constrained warping, which are given below:

$$\gamma_1^t = \gamma_{31}^t = \gamma_{31}^f - \gamma_{31}^p,
\gamma_2^t = \gamma_{32}^t = \gamma_{32}^f - \gamma_{32}^p.$$
(14)

The amplitude of warping in Eq. (4) can be expressed as $w = w_f - w_p$, where w_f is due to free (unconstrained) warping and w_p is associated with prevented (constrained) warping. The shear strains due to twisting from the free and constrained warping are rewritten as:

$$\gamma_{31}^{f} = \frac{\tau - T}{\lambda} \left(-S_2 + \frac{\partial \varphi}{\partial S_1} \right) = w_f \left(-S_2 + \frac{\partial \varphi}{\partial S_1} \right); \quad \gamma_{31}^{p} = w_p \frac{\partial \varphi}{\partial S_1},
\gamma_{32}^{f} = \frac{\tau - T}{\lambda} \left(S_1 + \frac{\partial \varphi}{\partial S_2} \right) = w_f \left(S_1 + \frac{\partial \varphi}{\partial S_2} \right); \quad \gamma_{32}^{p} = w_p \frac{\partial \varphi}{\partial S_1}.$$
(15)

The shear strains from twisting from Eqs. (14) and (15) are

$$\gamma_1^t = w_f \left(-S_2 + \frac{\partial \varphi}{\partial S_1} \right) - w_p \frac{\partial \varphi}{\partial S_1},
\gamma_2^t = w_f \left(S_1 + \frac{\partial \varphi}{\partial S_2} \right) - w_p \frac{\partial \varphi}{\partial S_2}.$$
(16)

For a slender beam, the transverse shear strains γ_1^s , γ_2^s are relatively small and often ignored. For an initially straight beam element with solid cross section, the axial strain in Eq. (12) reduces to:

$$\varepsilon = \varepsilon_{33} = \varepsilon_c - \frac{1}{\lambda} S_1 \kappa_2 + \frac{1}{\lambda} S_2 \kappa_1 \tag{17}$$

where ε_c is the axial strain of the centerline. With $\lambda \approx 1$, the axial stretch of the centerline can be dropped from Eq. (17).

The MDF panel is assumed linear elastic and isotropic with regard to its mechanical properties. The corresponding axial and shear stresses of the beam element are:

$$\sigma = E\varepsilon; \quad \tau_1 = G\gamma_1; \quad \tau_2 = G\gamma_2. \tag{18}$$

Finally, equilibrium equations are applied to the beam element, which are summarized below:

$$N = \int_{A_{o}} \sigma dA; \quad F_{1} = \int_{A_{o}} \tau_{1} dA; \quad F_{2} = \int_{A_{o}} \tau_{2} dA;$$

$$M_{1} = \int_{A_{o}} S_{2} \sigma dA; \quad M_{2} = -\int_{A_{o}} S_{1} \sigma dA; \quad T = \int_{A_{o}} (-S_{2} \tau_{1} + S_{1} \tau_{2}) dA;$$

$$W = \int_{A_{o}} \varphi (S_{1}, S_{2}) \sigma dA = 0$$
(19)

where N, F_1 , and F_2 are the axial (normal) force, shear force along S_1 axis, and shear force along S_2 axis, respectively, and A_0 is the cross-sectional area of the undeformed beam. The two bending moments rotating about the S_1 and S_2 axes are M_1 and M_2 , respectively, and the twisting moment rotating about the S_3 axis is T. It can be shown that for a solid rectangular cross section the bimoment W is zero. Also, for a rectangular cross section, the first moments of an area with respect to the S_1 and S_2 axes and the second moments of an area for cross-coupling in bending are zero. Thus, the equilibrium equations in Eq. (19) reduce to:

$$N = EA_{o}(\lambda - 1); \quad F_{1} = kGA_{o}\gamma_{1}^{s}; \quad F_{2} = kGA_{o}\gamma_{1}^{s};$$

$$M_{1} = EI_{11}\kappa_{1}; \quad M_{1} = EI_{22}\kappa_{2};$$

$$T = Gw_{f}I_{p} + GwJ$$
(20)

where $I_{11} = \int_{A_o} (S_2)^2 dA$ and $I_{22} = \int_{A_o} (S_1)^2 dA$ are the second moments of an area, $I_p = \int_{A_o} (S_1)^2 + (S_2)^2 dA$

is the polar moment of an area, and $J = \int_{A_0} (-S_2 \frac{\partial \varphi}{\partial S_1} + S_1 \frac{\partial \varphi}{\partial S_2}) dA$ is the torsional constant due to warping.

In Eq. (20), k is the correction factor for the transverse shear deformations from imposing uniform transverse shear stress and strain distributions instead of the actual nonlinear distributions. For a rectangular cross section, k = 5/6.

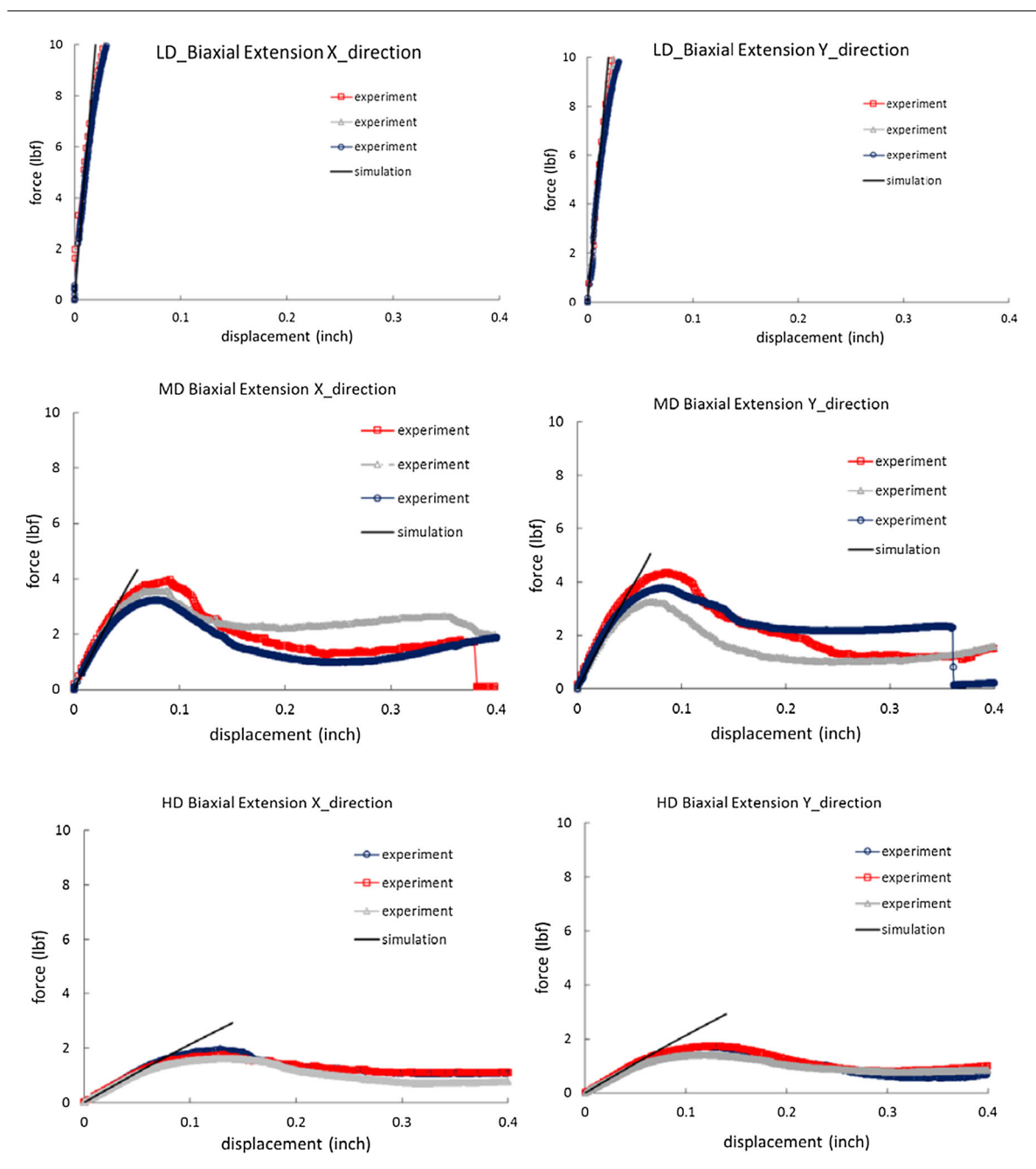


Fig. 12 Biaxial responses of the LD, MD, and HD square unit-cells

4.2 Simulation of unit-cell deformations

ABAQUS finite element (FE) analysis is considered for the deformations of the kerf unit-cells and panels. We first compare the responses analyzed using the beam element to those of using a three-dimensional (3D) continuum element, C3D8. The 3D continuum element allows for generating the unit-cell with precise shapes and sizes, including detailed model of the patterns. However, it can be computationally expensive, especially when one wants to generate a large-scale panel with complex deformed shapes. The use of beam elements will definitely reduce computational cost, especially when large-scale structural analyses are considered, with a caveat that precise geometrical shapes cannot be modeled. The B31 element in ABAQUS can incorporate axial stretching, transverse shearing, bending, and twisting of a noncircular cross section where warping can occur. We use the kerf unit-cells with MD cut to compare the force—displacement responses, mimicking the

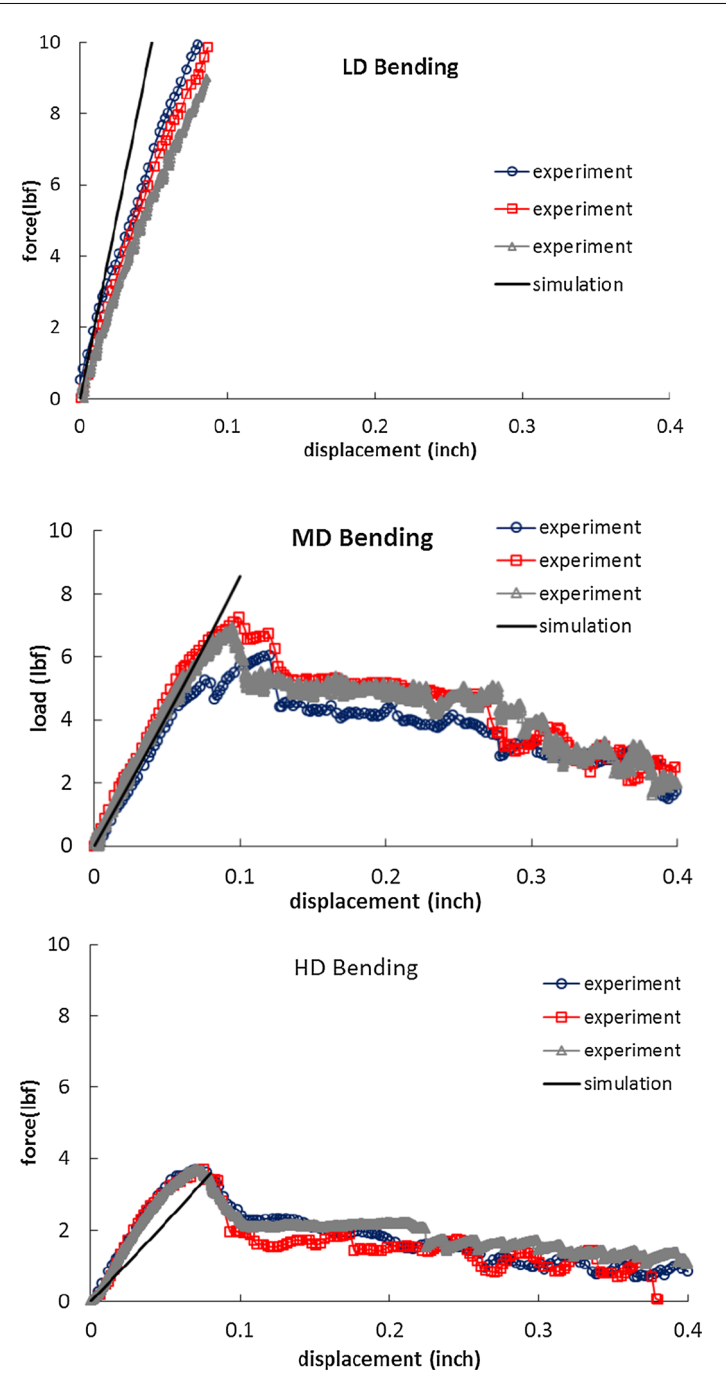


Fig. 13 Bending responses of square unit-cells

experiments, from the 3D continuum and beam elements (Figs. 8 and 9), which show a linear response. We determine the overall stiffness (force recorded divided by the prescribed displacement) to examine the responses under different loading conditions, i.e., axial and biaxial loadings and bending. Overall, the axial and biaxial responses from the beam and 3D elements match very well. Slight mismatches are seen in the bending behaviors. When the unit-cells are subjected to axial or biaxial loadings, the beam elements are dominated by bending about the out-of-plane (S_1) axis in which they can be adequately modeled as slender beams. When the unit-cell is subjected to bending, the beam elements are dominated by bending about the in-plane axis (S_2) and twisting. Bending about the in-plane axis occurs on a rather thick section, and hence, the transverse shear effects might not be negligible. Tables 1 and 2 summarize the cross-sectional dimensions,

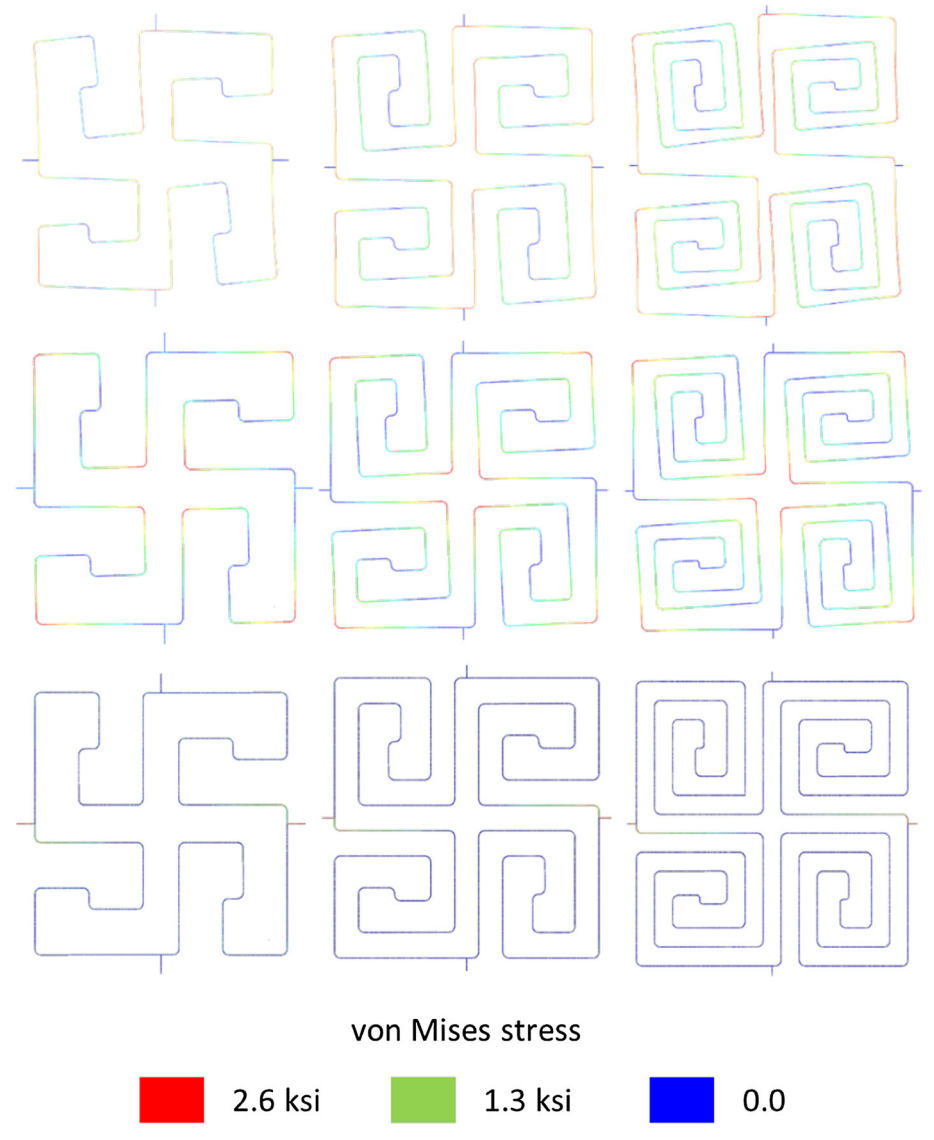


Fig. 14 Square cross section from beam model

second moments of an area, and polar moment of area of the beam elements in the unit-cells with different kerf patterns and cut densities. The material properties are discussed in Sect. 2. Further comparisons between the responses obtained from beam and continuum 3D elements for different loading conditions can be found in Chen [4], which shows a relatively small difference in the overall deformed shapes obtained from 3D continuum and beam elements.

The rest of the analyses will use beam elements in determining the deformations of the kerf unit-cell and panels. Figure 10 shows the beam element models for the unit-cells with different cut densities and kerf patterns. We also include the elements for the grip segments and prescribe the boundary conditions through these grip segments in order to mimic the experiments. Figures 11, 12, and 13 summarize the force—displacement responses of the square unit-cells with different cut densities (LD, MD, and HD) under uniaxial tension, biaxial tension, and bending, respectively. Overall, the simulations can capture the experimental responses, and deviations are seen for the bending cases. The simulations only consider linear elastic behaviors and do not include failure in the specimens. During loading, prior to visible damage, the force—displacement responses are fairly linear, and when a visible damage occurs the load continues to drop. Figure 14 illustrates the von Mises stress contours corresponding to the peak loading of the experiments. The stress indicates that there are regions with stress around or larger than 2.6 ksi, which is a failure stress of the MDF. The observed specimen failures

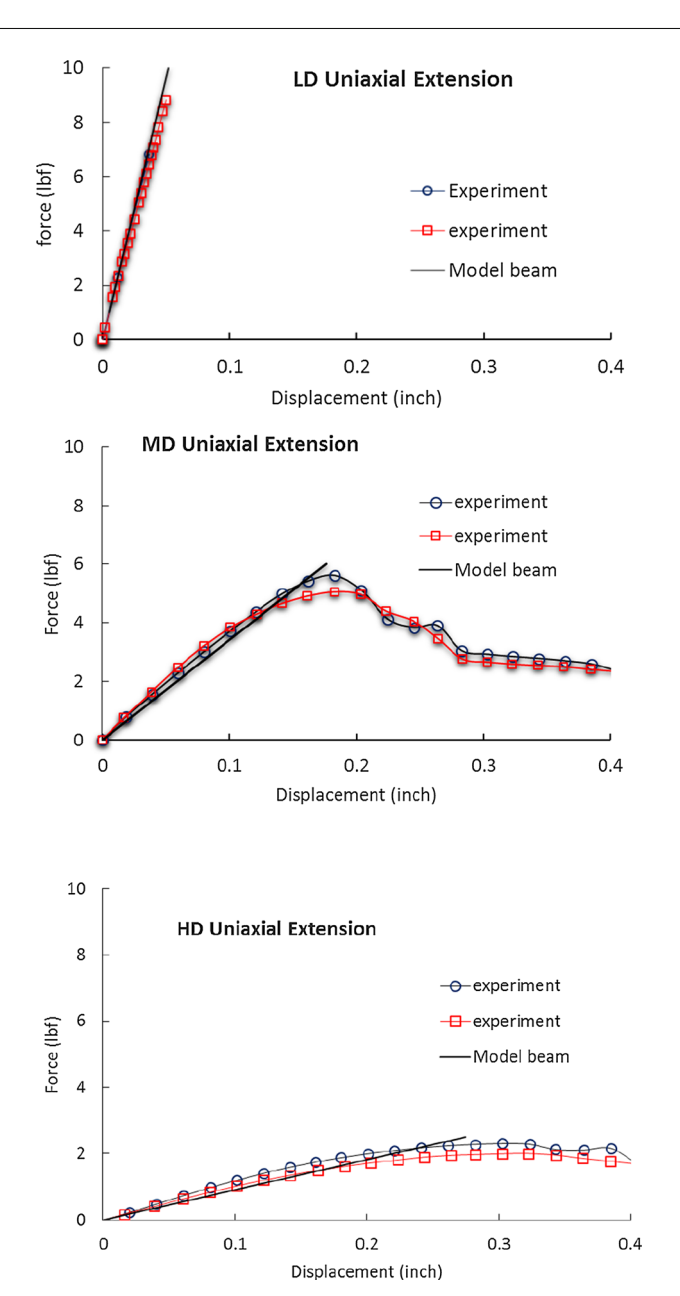


Fig. 15 Uniaxial responses of hexagonal unit cells

during testing are consistent with the stress patterns. In the uniaxial test, the specimen failed along the vertical bars in the middle of the unit-cell. In the biaxial test, the specimen failed at the four corners in the middle of the unit-cell. During the bending test, we observed that the push rod was not necessarily in contact with the four corners in the middle of the unit-cell, especially in the HD specimen. This might cause the slight mismatch between model and simulation. The mismatch in the bending response from the experiment and simulation from the LD specimens could be attributed to the rather short span of beam length (l) with large width (w), where l/w could be close to or less than one. In such situation, a beam element model is no longer applicable. This effect is quite negligible when the LD unit-cells were subjected to uniaxial and biaxial loadings since the deformations are mainly in the beams of relatively longer spans. To highlight the local deformations of beam segments in the unit-cell model under different loading conditions, Table 3 summarizes the deformations for the square unit-cell with MD cut. Under a uniaxial loading, the vertical beams are dominated by axial stretching, while the horizontal beams are undergoing in-plane bending and in-plane transverse shearing. For the biaxial loading, nearly all beam segments experience axial stretch, in-plane bending, and in-plane transverse shearing.

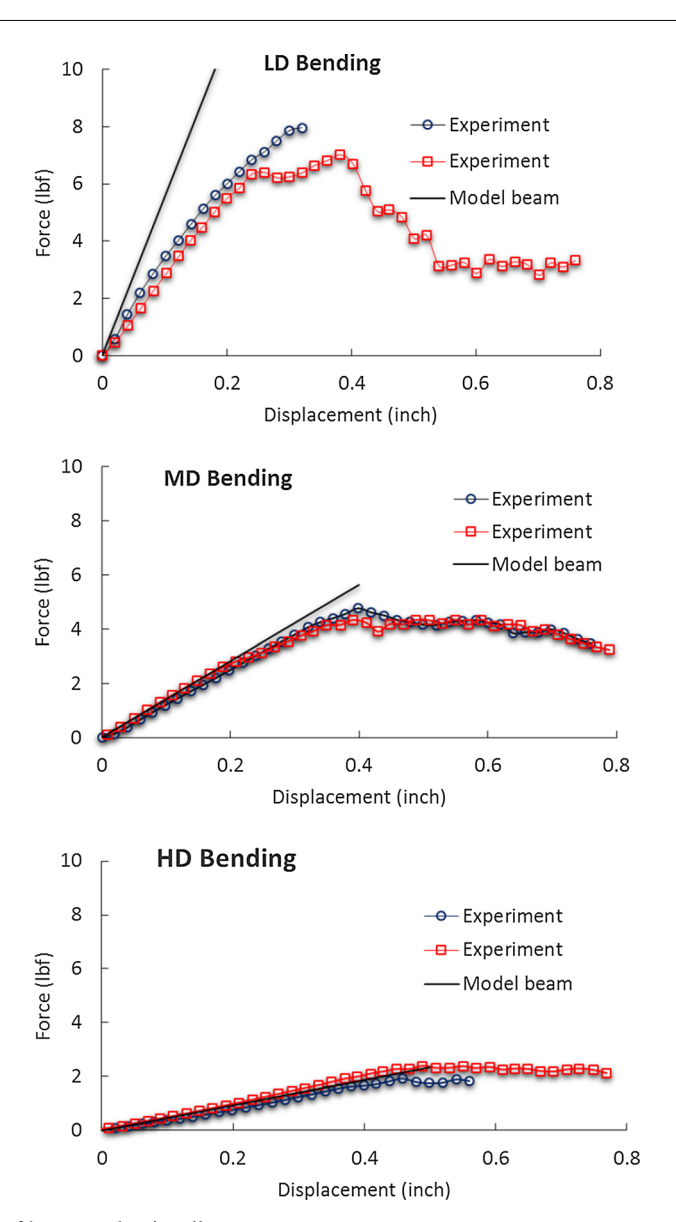


Fig. 16 Bending responses of hexagonal unit cells

Under a bending condition, in which the unit-cell is constrained at the two ends along the *x*-axis and out-of-plane lateral deformation is prescribed to the four central corners, some of the beam segments experience out-of-plane bending and out-of-plane transverse shearing while other beam segments undergo out-of-plane bending and twisting.

Figures 15 and 16 show the responses from the hexagon unit-cells with different cut densities. Again, the beam elements can capture the overall deformations of the unit-cells, except for bending of the LD unit-cell. Figure 17 depicts the von Mises stress contour from the uniaxial tension (top) and bending (bottom). We also observed that failure in the specimens during testing is consistent with the regions of high stresses. As expected, the cut with higher density gives more flexible deformations due to significantly low second moments and polar moment of an area of each beam segment between the cut lines. Adding more cut lines will certainly create more flexible structures. However, increasing cut lines leads to smaller area of each beam segment between the cut lines, hence reducing load carrying capability of the overall structures. Similar to the square unit-cell response, the simulation shows linear behaviors, which are attributed to the use of a linear elastic constitutive model for the beam element model. The experiments show linear responses only up to a certain load level, and nonlinear responses are seen followed by failure of the specimens.

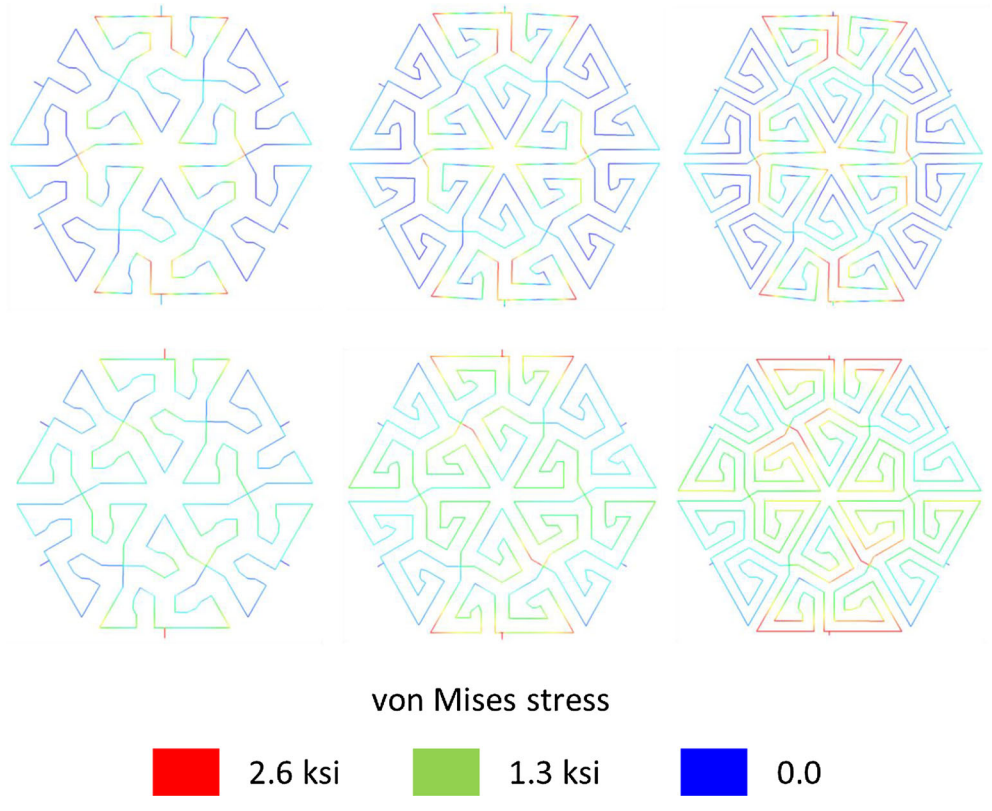


Fig. 17 Hexagonal patterns from beam model

We summarize the overall stiffness (force/displacement) from the unit-cells of square and hexagon patterns with different cut densities and under various loading conditions, as shown in Figs. 18 and 19. As expected, higher density cut leads to more compliant responses, as indicated by low stiffness. The hexagon patterns yield more flexible responses compared to the square patterns. This is due to more cut lines in the hexagon unit-cells, and hence, rather slender beam elements are used to form the hexagon unit-cells. We also compared the stiffness from the experimental and numerical results. Overall, they agree well, except that large mismatches are seen for LD unit-cells under bending, as described above. When designing a kerf panel, regions with LD cuts are generally under very low or negligible deformations, and LD cuts are often used to generate smoother transitions within the panel. Under very small deformations, the beam elements can capture the deformations in the LD unit-cells under all loading conditions.

4.3 Designing freeform shapes an MDF kerf panel

Based on the understanding of the unit-cell deformations, we can design kerf panels of complex geometries (freeform structures). As noted from the unit-cell studies, higher cut densities lead to more flexible systems that are easily deformed to complex shapes, but they experience larger stresses, reducing the load bearing ability of the systems. In designing kerf panels for generating freeform shapes, we can vary the cut densities within the panels, i.e., regions with high curvatures will require high-density cuts. If we restrict the design to developable surfaces from a planar surface, which is done by an isometric mapping, then the surfaces can be achieved without local distortion or cutting. In the developable surfaces, in which the Gaussian curvature is zero, we can achieve the shapes without inducing distortion and hence no stresses induced to the beam segments. When the surfaces are not developable, indicated by nonzero Gaussian curvatures, it is then necessary to examine the stresses in the beam segments of the kerf panels and redesign the shape accordingly in order to avoid regions with over-stressed conditions. We present two cases of simple surfaces with nonzero and zero Gaussian curvatures as to illustrate the advantage of dealing with developable surfaces, the consequence of non-developable surfaces, and the corresponding stresses in the beam segments in both cases.

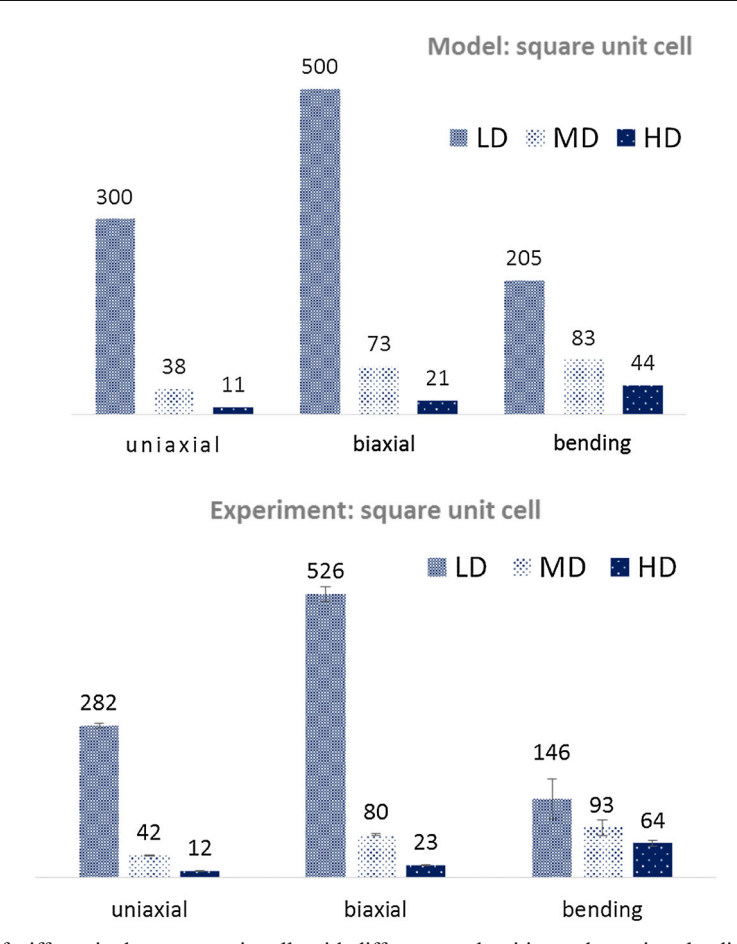
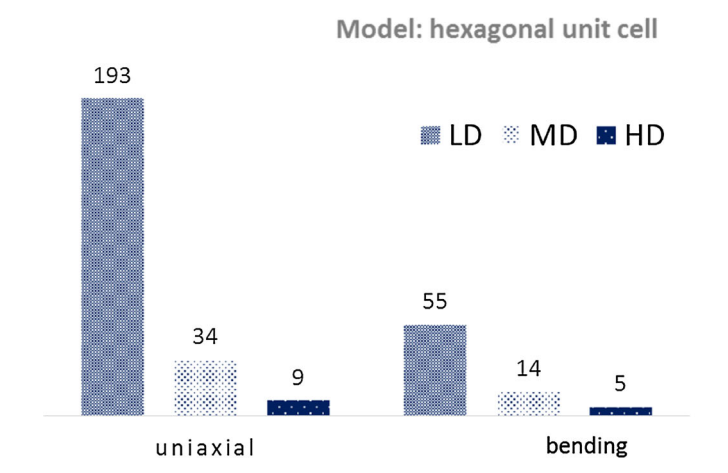


Fig. 18 Comparisons of stiffness in the square unit-cells with different cut densities under various loadings from simulation (top) and experiment (bottom)

The desired freeform shapes can be determined by defining a mapping function $\chi(X)$ that maps a particle at a position X in the undeformed state to the deformed state x. From the mapping function, we can define various measures of curvatures and the corresponding deformation gradient $F = \frac{\partial \chi(X)}{\partial X} = \frac{\partial x}{\partial X}$. Once the deformation gradient is obtained, the corresponding strain measures and hence stresses in the kerf panel can be calculated, see a similar discussion in Sohrabi et al. [22] for truss systems. In a relatively thin plate, large deformations are dominated by large rotation while the plate experiences relatively small strains [2,5,13,23]. In this study, we attempt to design kerf panels of specific shapes while keeping the maximum stresses way below 2.6 ksi (the failure stress of the MDF). We present surface geometry analyses as a first step to examine the type of surfaces, whether they are developable measured by zero Gaussian curvature. The corresponding surfaces out of kerf panels are then modeled using the beam elements, and we further study the corresponding stresses in the beam elements of the deformed kerf panels.

Consider an initially flat surface with in-plane dimensions defined by X_1 and X_2 axes and the out-of-plane direction defined by X_3 axis. Given an explicit function for the out-of-plane displacement that determines a freeform shape $u_3 = h(X_1, X_2)$, we can compute the principal curvatures (κ_1, κ_2) and also the Gaussian curvature $\kappa_G = \kappa_1.\kappa_2$ within the freeform shape. When the Gaussian curvature is equal to zero, the panel can be deformed to the freeform shape without distorting it, i.e., no stretching and tearing of the material, and hence, the stresses within this freeform surface will be equal to zero. When the Gaussian curvature within the freeform shape is nonzero, we then need to determine the maximum stresses in the surface and redesign the shapes in order to meet the maximum stress limit.



Experiment: hexgonal unit cell

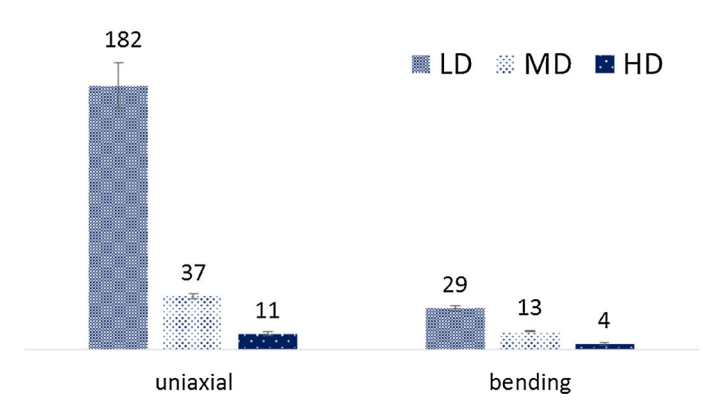


Fig. 19 Comparisons of stiffness in the hexagon unit-cells with different cut densities under various loadings from simulation (top) and experiment (bottom)

The principal curvatures are determined as follows:

$$\kappa_{1}, \kappa_{2} = H \pm \sqrt{H^{2} - K},
H = \frac{\left(1 + h_{1}^{2}\right) h_{22} - 2h_{1}h_{2}h_{12} + \left(1 + h_{2}^{2}\right)h_{11}}{2\left(1 + h_{1}^{2} + h_{2}^{2}\right)^{3/2}},
K = \frac{h_{11}h_{22} - h_{12}^{2}}{\left(1 + h_{1}^{2} + h_{2}^{2}\right)^{2}},
h_{1} = \frac{\partial h\left(X_{1}, X_{2}\right)}{\partial X_{1}}; \quad h_{2} = \frac{\partial h\left(X_{1}, X_{2}\right)}{\partial X_{2}};
h_{11} = \frac{\partial^{2}h\left(X_{1}, X_{2}\right)}{\partial X_{1}^{2}}; \quad h_{22} = \frac{\partial^{2}h\left(X_{1}, X_{2}\right)}{\partial X_{2}^{2}}; \quad h_{12} = \frac{\partial^{2}h\left(X_{1}, X_{2}\right)}{\partial X_{1}\partial X_{2}}. \tag{22}$$

We present two examples of rather simple freeform shapes, i.e., dome and saddle shapes, in order to clearly illustrate the design and analysis of kerf panels in generating freeform structures.

1. Dome shape

The dome shape is formed by the following mapping function:

$$x_1 = X_1; \quad x_2 = X_2; \quad x_3 = X_3 + e^{-A[(X_1)^2 + (X_2)^2]}, -L_1/2 \le X_1 \le L_1/2; \quad -L_2/2 \le X_2 \le L_2/2$$
(23)

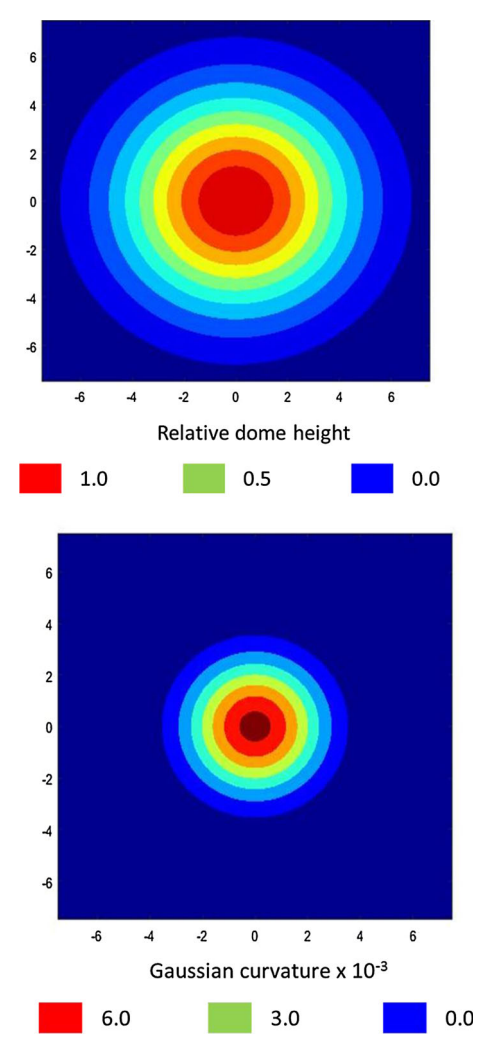


Fig. 20 Dome amplitude and Gaussian curvature

where L_1xL_2 is the planar dimension of the flat surface, and A is a constant that determines the sharpness of the dome. Let us consider a flat panel of 15×15 , inches and with A = 0.04, the dome shape, and corresponding Gaussian curvature is shown in Fig. 20. The nonzero values of the Gaussian curvature are mostly in the center region of the panel. In designing the kerf panel to create the dome shape, we consider a square pattern. The HD cut is used for the regions of high curvature ($\kappa_G > 10^{-3}$) while regions with zero curvature are designed with LD cut. We also consider transition regions from LD to HD with the MD cut. Figure 21 top shows the cut density distribution in a kerf panel with a square pattern that will be deformed into a dome shape. The kerf panel out of MDF with the corresponding cut density distribution is shown in Fig. 5. In this study, determining the curvature threshold for the cut density distribution is rather arbitrary, and the cut densities are placed manually. In the future, we plan to automatically generate the desired freeform shapes, the corresponding kerf patterns, and the cut density distributions that meet the design criteria.

The kerf panel is then subjected to a bending deformation to generate the dome shape by applying out-of-plane displacement to the center of the panel, corresponding to the mechanical test in Fig. 5. Figure 21 middle depicts the out-of-plane force—displacement responses from experiment and simulation. The corresponding von Mises stress contour is also shown in Fig. 21 bottom. The dome amplitude is limited in order to avoid a nonlinear material response and failure. A slight stiffening in the response is attributed to the deformations of the HD cut at early loading, followed by the deformation in the MD cut at later stage of loading. The regions of LD cut experience no deformation, as expected. A dome shape out of a hexagon pattern is depicted in Fig. 22. Similarly, the dome amplitude is limited so that the maximum stresses in the beam elements are much smaller than the failure stress of the MDF. The force—displacement response from the simulation is comparable to the experimental result. At a larger displacement, a deviation in the model and experiment is seen. The stiffening

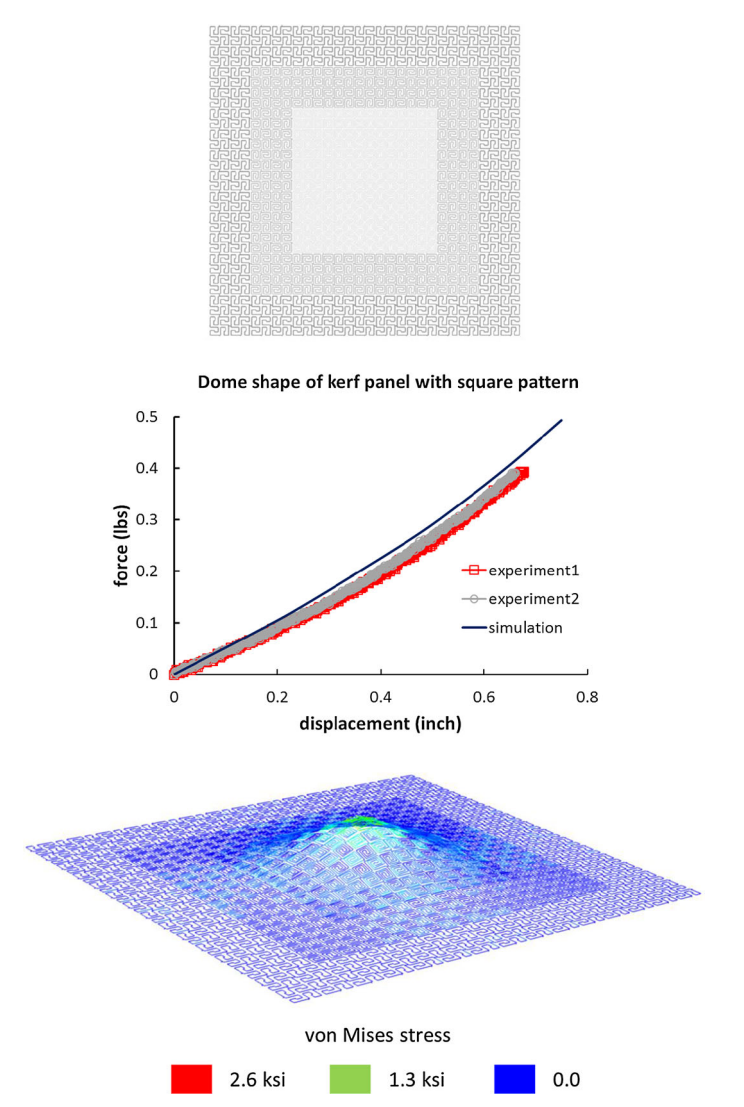


Fig. 21 Dome shape of a kerf panel with a square pattern. Top: panel with different cut densities; middle: the load–displacement response; bottom: von Mises stress contour

in the experiment at larger displacement is associated with the contact of six center tips of the kerf segments which is not seen in the square pattern. The model does not include any contact surfaces.

2. Saddle shape

The saddle shape is obtained from the following mapping function:

$$x_1 = X_1; \quad x_2 = X_2; \quad x_3 = X_3 + AX_1X_2$$

- $L_1/2 \le X_1 \le L_1/2; \quad -L_2/2 \le X_2 \le L_2/2.$ (24)

With A=1, the principal curvatures and Gaussian curvature are determined, as summarized in Fig. 23. It is seen that to achieve the saddle shape with the mapping function in Eq. (24), the panel can be deformed without inducing any distortion to the material, and hence, the stresses will be zero. This is in accordance with the zero Gaussian curvature. Unlike in the dome shape, we cannot use the Gaussian curvature to determine the distribution of cut densities within the panel, we consider another geometrical measure that depends on the gradient of the out of plane displacement $\kappa_T = (\frac{\partial h}{\partial X_1})^2 + (\frac{\partial h}{\partial X_2})^2$. Figure 24 shows the saddle shape displacement from the mapping function in Eq. (24) and the corresponding parameter κ_T . The parameter κ_T will be used to distribute the cut densities within the panel. The regions with high values (> 500) will have HD cut, and regions with low values (< 50) will have LD cut,

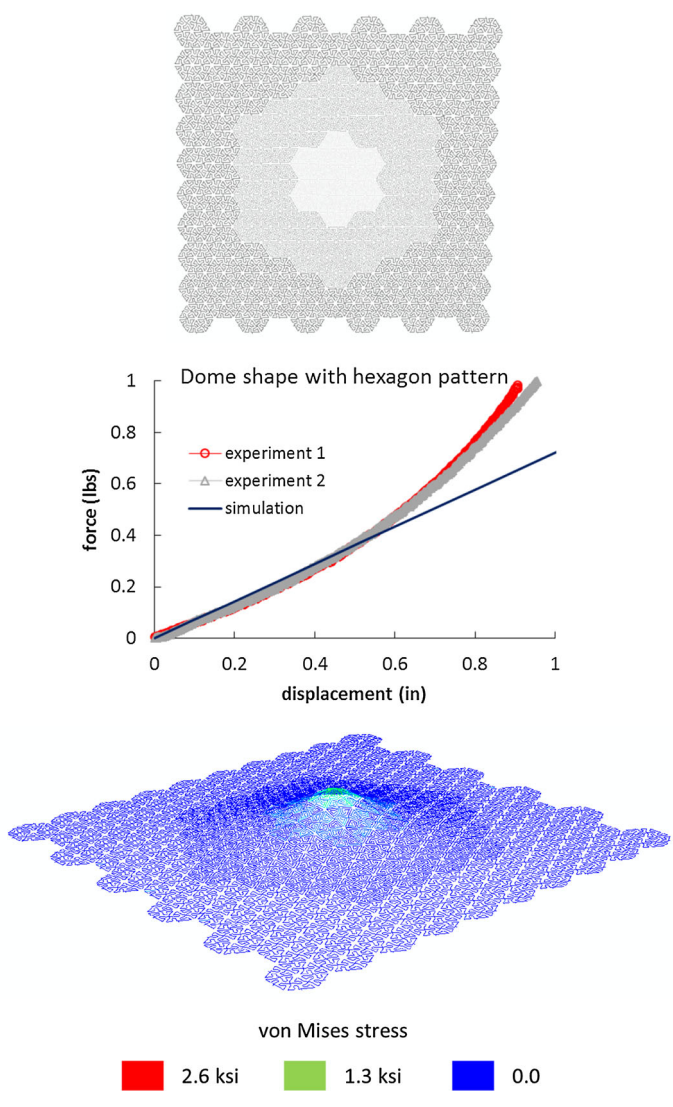


Fig. 22 Dome shape of a kerf panel with a hexagon pattern. Top: panel with different cut densities; middle: the load–displacement response; bottom: von Mises stress contour

and the remaining will be with MD cut. The cut densities are also shown in Fig. 24. The saddle shape that is formed by the kerf panel is shown in Fig. 25. It is seen that the von Mises stresses are zero throughout the panel, except small values close to the locations where loads are prescribed.

It is noted that we use the Gaussian curvature κ_G and another geometrical parameter κ_T of surfaces to manually estimate locations in the kerf panel with HD cuts and examine the capability of the beam element models in estimating the overall deformations of the kerf panels. In the future, we plan to include an optimization method to our kerf panel analyses in order to automatically generate the desired freeform shapes and their corresponding kerf patterns and cut density distributions that meet the design criteria.

5 Conclusions

We have presented experimental work and simulation on understanding the mechanical responses of kerf panels. Unit-cells of two kerf patterns, i.e., square and hexagon, out of MDF with different cut densities have been subjected to uniaxial and biaxial stretching and out-of-plane bending. The mechanical responses of the kerf unit-cells were simulated using a beam element model that accounts for axial, bending, twisting, and transverse shear deformations. A linear elastic constitutive material model was considered for the beam model.

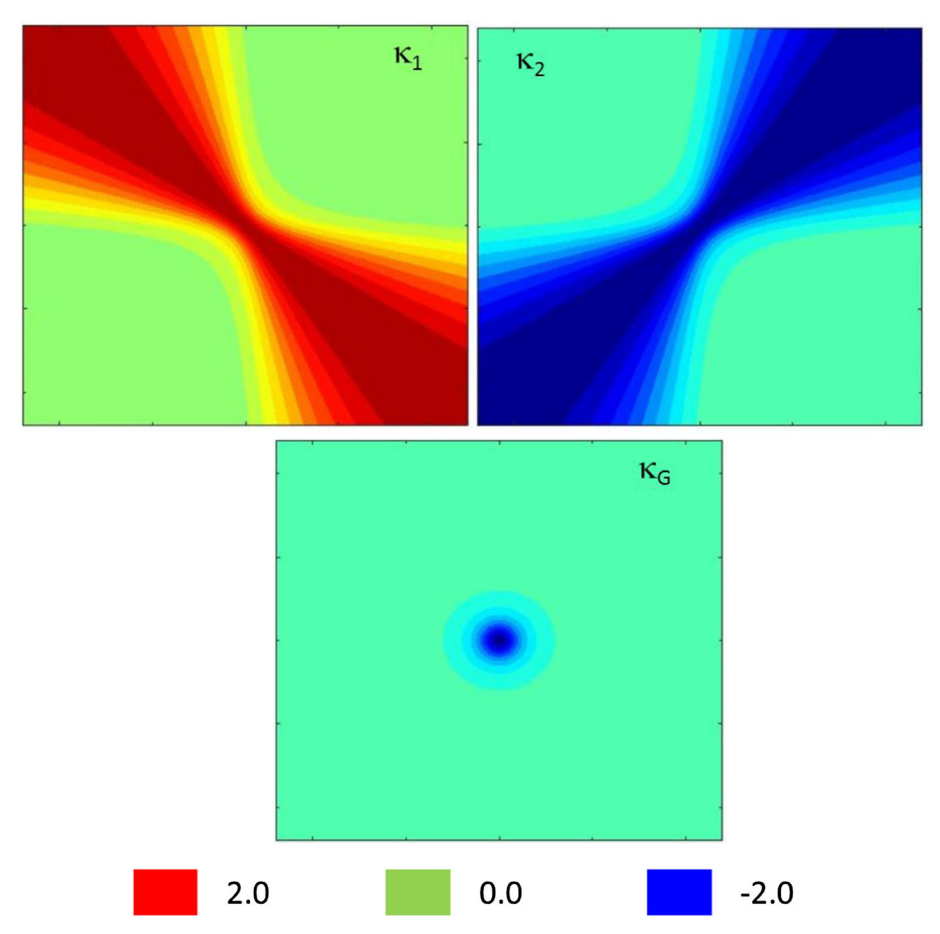


Fig. 23 Saddle shape curvature measures

The simulations can capture the responses of the unit-cells under different loading conditions. As expected, the beam element model shows linear responses of the unit-cells, and the nonlinear responses in the experiments are associated with damage and breaking of the specimens. Furthermore, we have tested and simulated a dome shape of kerf panels with square and hexagon patterns. Again, the responses from simulation and experiment correlate well.

In the low-density cut of unit-cell models, both for square and hexagon patterns, mismatches in the bending response from experiment and simulation are observed. In the low-density cut, the segments in the kerf pattern about the bending axis are quite stocky, in which beam elements are not suitable in capturing their deformations. The low-density cuts give the stiffest responses for all loading conditions when compared to the medium and high-density cuts, which are expected. In designing kerf panels of freeform shapes, the use of low-density cuts will be in the regions of very low curvatures, and they are mostly used for improving load bearing.

We have also demonstrated the design and analysis of simple shapes of the panels, of dome and saddle shapes, using the kerfing method in order to highlight the differences in the deformation behaviors between developable and non-developable surfaces. We have presented arrangements of cut densities in achieving the desired shapes. It is also noted that in case the Gaussian curvature of the panel is zero, i.e., in the saddle shape, the kerf panel can be deformed without inducing any stresses, which should be expected. The kerfing technique is not limited to only achieving simple shapes, it can be easily deformed to more complex shapes. In addition, a continuous transition in cut densities can also be achieved by parameterizing multiple design variables. In the future, an optimization method will be incorporated to the kerf panel analyses in order to automatically generate the desired freeform shapes and their corresponding kerf patterns and cut density distributions that meet the design criteria.

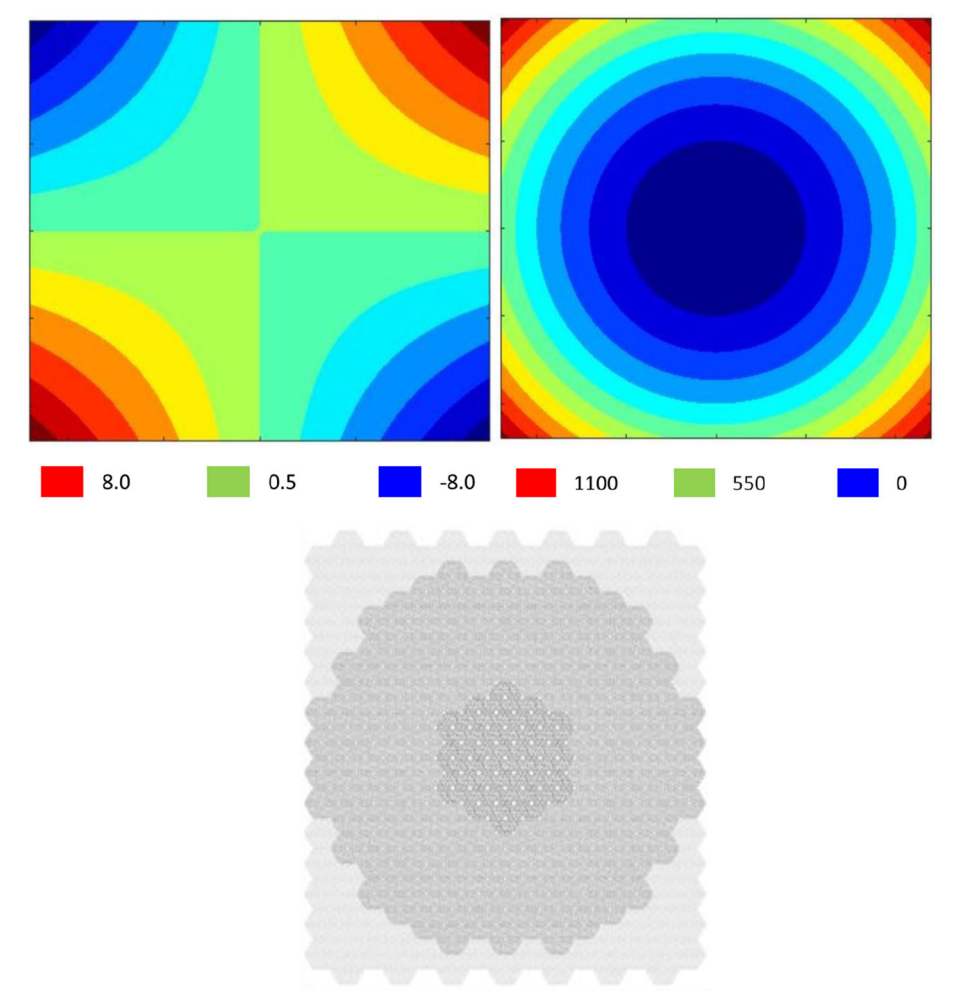


Fig. 24 Saddle shape displacement (top left), curvature κ_T measure (top right), and cut pattern (bottom)

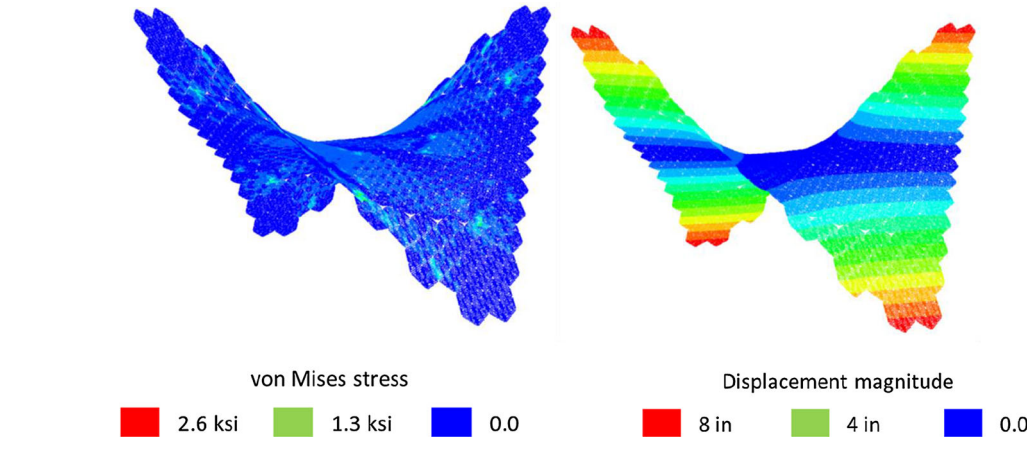


Fig. 25 von Mises stress (left) and displacement (right)

References

- 1. Andrade, D., Harada, M., Shimada, K.: Framework for automatic generation of facades on free-form surfaces. Front. Archit. Res. 6, 273–289 (2017)
- Cai, Y.C., Atluri, S.N.: Large rotation analyses of plate/shell structures based on the primal variational principle and a fully nonlinear theory in the updated Lagrangian co-rotational reference frame. CMES: Comput. Model. Eng. Sci. 83, 249–273 (2012)
- 3. Cesarek, P., Saje, M., Zupan, D.: Kinematically exact curved and twisted strain-based beam. Int. J. Solids Struct. 49, 1802–1817 (2012)
- 4. Chen, R., Jiang, M., Kalantar, N., Moreno, M., Muliana, A.: "Creating flexible structures out of MDF Plates" 33rd ASC Technical Conference, University of Washington (Sept 2018)
- 5. Crisfield, A., Moita, G.F.: A unified co-rotational framework for solids, shells and beams. Int. J. Solid Struct. 33, 2969–2992 (1996)
- Greenberg, E., Korner, A.: Substractive manufacturing for variable-stiffness plywood composite structures. Sustain. Des. Manuf. sdm14–036, 50–66 (2014)
- 7. Guseinov, R., McMahan, C., Perez, J., Daraio, C., Bickel, B.: Programming temporal morphing of self-actuated shells. Nat. Commun. 11, 237 (2020)
- 8. Guzelci, O.Z., Alacam, S., Bacinoglu, S.Z.: Three-step experimentation on embedding curvature to rigid planar materials through cut patterns. Gestão e Tecnol. de Proj. São Carlos 12(3), 93–107 (2017). https://doi.org/10.11606/gtp.v12i3.134543
- 9. Hoffer, B., Kahan, G., Crain, T., Miranowski, D.: Kerf Pavilion (2012). https://architecture.mit.edu/architecture-and-urbanism/project/kerf-pavilion
- 10. Ivanišević, D.: Super flexible laser cut plywood (2014). http://lab.kofaktor.hr/en/portfolio/super-flexible-laser-cut-plywood
- 11. Irschik, H., Gerstmayr, J.: A continuum mechanics based derivation of Rreissner's large displacement finite strain beam theory: the case of plane deformations of originally straight Bernoulli-Euler beams. Acta Mech. 206, 1–21 (2009)
- 12. Kalantar, N., Borhani, A.: Informing deformable formworks, parameterizing deformation behavior of a non-stretchable membrane via kerfing. In: Learning, Prototyping and Adapting—Proceedings of the 23rd CAADRIA Conference—Volume 2, Tsinghua University, Beijing, China, 17–19 May 2018, pp. 339–348 (2018)
- 13. Kang, L., Zhang, Q.L., Wang, Q.L.: Linear and geometrically nonlinear analysis of novel flat shell elements with rotational degrees of freedom. Finite Elem. Anal. Des 45, 386–392 (2009)
- 14. Konakovic-Lukovic, M., Panetta, J., Crane, K., Pauly, M.: Rapid deployment of curved surfaces via programmable auxetics. ACM Trans. Gr. 37, 106 (2018)
- 15. Muliana, A.H.: Large deformations of nonlinear viscoelastic and multi-responsive beams. Int. J. Nonlinear Mech. 71, 152–164 (2015)
- 16. Postle, B.: Methods for creating curved shell structures from sheet materials. Buildings 2, 424–455 (2012)
- Pottmann, H., Liu, Y., Wallner, J., Bobenko, A., Wang, W.: Geometry of multi-layer freeform structures for architecture. ACM Trans. Gr. 26(65), 1–11 (2007)
- 18. Reissner, E.: On one-dimensional finite strain beam theory. J. Appl. Math. Phys (ZAMP) 23, 795-804 (1972)
- 19. Saje, M., Srpcic, S.: Large deformations of in-plane beam. Int. J. Solids Struct. 21, 1181–1195 (1985)
- Simo, J.C.: A finite strain beam formulation. the three-dimensional dynamic problem part I. Comput. Methods Appl. Mech. Eng. 49, 55–70 (1984)
- 21. Sliseris, J., Andra, H., Kabel, M., Dix, B., Plinke, B.: Virtual characterization of MDF fiber network. Eur. J. Wood Prod. 75, 397–407 (2017)
- 22. Sohrabi, A., Muliana, A., Srinivasa, A.: Controlling deformation in electro-active truss structures with nonlinear history-dependent response. Finite Elem. Anal. Des. 129, 42–52 (2017)
- Tajeddini, V., Muliana, A.: Deformation of flexible and foldable electro-active composite structures. Compos. Struct. 160, 280–291 (2017)
- 24. Zarrinmehr, S., Ettehad, M., Kalantar, N., Borhani, A., Sueda, S., Akleman, E.: Interlocked archimedean spirals for conversion of planar rigid panels into locally flexible panels with stiffness control. Comput. Gr. 66, 93–102 (2017)
- 25. Zehnder, J., Knoop, E., Bacher, M., Thomaszewski, B.: Metasilicone: design and fabrication of composite silicone with desired mechanical properties. ACM Trans. Gr. 36, 240 (2017)

Publisher's Note Springer Nature remains neutral with regard to jurisdictional claims in published maps and institutional affiliations.